Pulsations Along Stellar Evolution
VIII LAPIS Summer School
AAA Workshop Series 12, 2021
M. Kraus & A.F. Torres, eds.

Pulsations in Evolved Massive Stars

M. Kraus[1]

[1] *Astronomical Institute, Czech Academy of Sciences, Fričova 298, 251 65 Ondřejov, Czech Republic*

Abstract. The post-main sequence evolution of massive stars still bears many unknowns. In particular, the physical processes involved in triggering enhanced mass-loss or eruptions are yet to be established. In this Chapter, the post-main sequence evolution of massive stars, and the various phases which are well-known for their mass ejections, are briefly touched upon. Amongst those transition phases, two classes of objects are discussed in more detail: the B-type supergiants and the Yellow Hypergiants. Their ability to perform pulsations is presented based on observational and theoretical evidences. Moreover, the possibility of a pulsation–mass-loss relation in these two classes of objects is delineated.

Key words: asteroseismology — instabilities — stars: oscillations — stars: winds, outflows

1. Introduction to Massive Stars

Massive stars are stars that are born with initial masses $> 8\,M_\odot$. They are few in numbers, but their significance lies in their powerful winds with which they enrich their environments throughout their entire life in both momentum and chemically processed material. With their enormous energy transfer, in particular during their explosion as powerful supernovae, massive stars may trigger the formation of next generations of stars and planets. Consequently, they play a crucial role in the dynamical and chemical evolution of their host galaxies. It is therefore surprising that stellar evolution theory is still most uncertain for massive stars, despite their importance.

1.1. Evolution of Massive Stars - Theoretical Aspects

From a theoretical point of view, the various phases in the life of a massive star are clearly defined, namely in terms of the individual nuclear burning stages. On the main-sequence, the star burns hydrogen in its core into helium. As soon as the hydrogen core is exhausted, the star turns off the main-sequence and performs pure hydrogen shell-burning in a layer around the core, whereas the core itself contracts and heats until helium burning sets in. This sequence of core and shell burning into heavier and heavier elements continues until the core consists only of the iron ashes. In this final pre-supernova stage, the iron core is surrounded by multiple shell-burning layers, of which the hydrogen-burning layer is closest to the stellar surface, underneath the outermost, non-burning stellar hydrogen envelope.

From stellar evolution theory, all these individual burning phases can be unambiguously determined and chronologically ordered. However, these phases refer purely to the properties inherent to the stellar interior. They are not directly accessible by observations. Moreover, stars can rotate and undergo strong mass-loss, influencing and altering significantly the internal structure and surface appearance of massive stars.

Stellar Winds An excellent introduction into the subject of stellar winds is provided by the textbook of Lamers & Cassinelli (1999). Here, only some general aspects are briefly outlined.

Multiply ionized elements can have excited states with extremely short lifetimes. If such a state is excited due to the absorption of a photon, the deexcitation happens quasi instantaneously. Lines of such transitions are called resonance lines. Based on their energies, these resonance lines typically arise within the ultraviolet spectral range.

Ions of various elements in the upper atmosphere of a hot, massive star can produce resonance lines. These ions continuously absorb photons from the underlying photosphere into their resonance states. The re-emission occurs into the solid angle 4π, resulting in a net momentum transfer from the photospheric photons to the ions in predominantly radial direction. Consequently, the ions experience a constant radial "push" and as such an acceleration beyond the sonic point. Collisions between these accelerated ions and other elements and free electrons in their vicinity drag these particles along, leading to a global removal of matter from the stellar surface known as mass-loss via line-driven winds. Depending on the physical properties of the star, the mass-loss during some evolutionary phases can be so high, that the outer layers of the star are completely peeled off. If this happens, deeper layers, which are enriched in heavier elements due to shell-burning processes, show up on the stellar surface, and the star appears "stripped".

Stellar Rotation Rotation in the interior of stars can lead to mixing and hence transportation of chemically processed material from deeper layers to the stellar surface. But rotation has also another effect: it can deform the shape of the star. With increasing rotation speed stars loose their spherical shape and instead appear flattened. The best known rotating body that displays a deviation from spherical symmetry is the Earth with its equatorial radius exceeding the polar one by about 21 km, corresponding to a flattening of 0.00335.

The parameter $\omega = v_{\rm rot,eq}/v_{\rm crit}$ defines the ratio between the equatorial rotation velocity, $v_{\rm rot,eq}$, and the critical velocity, $v_{\rm crit}$. The latter is given by $v_{\rm crit} = \sqrt{GM_{\rm eff}/R_{\rm eq}}$, where G is the gravitational constant, $M_{\rm eff}$ is the effective stellar mass, i.e. the stellar mass reduced by the effects of radiation pressure due to electron scattering, and $R_{\rm eq}$ is the stellar radius at the equator. Critical rotation is reached if $\omega = 1$, meaning that the centrifugal force balances the gravitational force. In this case, $R_{\rm eq} = 1.5R_{\rm pole}$, where $R_{\rm pole}$ is the radius at the pole, and a maximum flattening of $(R_{\rm eq} - R_{\rm pole})/R_{\rm pole} = 0.5$ is reached.

The deformation of the stellar shape has a further consequence. The compression of the polar regions results in a heating of the poles, whereas the expansion of the equatorial regions leads to a cooling. This effect is also known as gravitational darkening. The gradient in surface temperature from the pole

to the equator leads also to a latitude dependence of the mass flux. As long as no change in the ionization state of the wind material occurs from the polar to the equatorial region, rotating stars tend to have higher mass flux over the poles and less mass flux along equatorial regions (see Figure 2 in Kraus, 2006). The situation may be different in rapidly rotating stars, in which the ionization state of the gas in the wind can change at a certain latitude due to the drastic drop in surface temperature. For such stars higher mass flux may be expected in equatorial regions due to the increased number of ions suitable for line-driving. This effect is known as the rotation induced bi-stability mechanism (Pelupessy et al., 2000). Moreover, the star may switch from the classical fast solution (Castor et al., 1975) to the so-called slow solution (Curé, 2004) leading also to increased mass-loss in equatorial regions.

The real rotation speed of a star is difficult to guess, because usually the inclination of the rotation axis is not known. Therefore, observations typically deliver only $v_{\rm rot,eq} \sin i$, i.e. the rotation velocity projected to the line-of-sight, which is a *lower limit* to the real rotation velocity. Estimates of projected rotation velocities for massive single-star non-supergiant samples, performed in the Tarantula (30 Dor) nebula of the Large Magellanic Cloud, revealed a velocity distribution with a strong peak at low values ($\sim 80\,{\rm km\,s^{-1}}$) and a high-velocity tail (up to $600\,{\rm km\,s^{-1}}$) for O-type stars ($16-60\,{\rm M_\odot}$, Ramírez-Agudelo et al., 2013), whereas B-type stars ($8-16\,{\rm M_\odot}$, Dufton et al., 2013) can show a bi-modal distribution with a significant fraction of stars having projected rotation velocities $< 100\,{\rm km\,s^{-1}}$ and another peak spreading from 200 to $250\,{\rm km\,s^{-1}}$. Also for these type of stars a high-velocity tail (up to $\sim 500\,{\rm km\,s^{-1}}$) is observed, meaning that a small fraction of O and B-type stars are born with intrinsic rotation speeds corresponding to a significant fraction of their critical velocities.

A deeper discussion of the effects of rotation on the physics and evolution of massive stars is provided by the excellent textbook of Maeder (2009).

Evolutionary Tracks To predict the properties of massive stars along their entire life path, various research groups have developed their own computer codes (see Martins & Palacios, 2013, for an overview). All these codes are pure one-dimensional and utilize a variety of input physics that is implemented in different ways. Computation of evolutionary tracks of massive stars is performed from the point of ignition of hydrogen in the stellar cores, defined as the zero-age main-sequence (ZAMS), up to pre-supernova stages. But comparison of the model predictions for the evolutionary track of a massive star with initially identical properties clearly shows a huge diversity and strong disagreement, especially after the star turns off from the main sequence. This was impressively demonstrated by the analysis of Martins & Palacios (2013) (see, e.g., their Figure 4).

Moreover, both effects, rotation and mass-loss, significantly influence and alter the evolution of massive stars as previously discussed. Rotation drives the internal mixing and influences mass-loss rates already on the main-sequence. Consequently, stars with initially identical masses on the ZAMS but diverse rotation velocities will end up with different properties when they reach the end of their main-sequence evolution (Meynet & Maeder, 2000).

Given the uncertainties in stellar models and in the (usually poorly constraint) initial physical properties such as rotation, it is tricky to assign a star a

proper initial mass and evolutionary state from a pure comparison of its position in the Hertzsprung-Russell (HR) diagram with evolutionary model predictions.

1.2. Observed Spectroscopic Phases

From the observational point of view, massive stars in their post-main sequence evolution are classified based on their spectroscopic appearance. In general, one distinguishes two types of objects: supergiants and hypergiants.

Supergiants are stars of luminosity class I with subclasses Ia, Iab, and Ib. In the HR diagram they spread from the hottest to the coolest stars and are classified according to their effective temperature into blue supergiants (spectral types O and B), yellow supergiants (A, F, G), and red supergiants (K, M).

Objects in the category hypergiants spread also over a certain temperature range in the HR diagram. Known hypergiants have spectral types ranging from late-O to G. Hypergiants are often assigned a luminosity class 0 or Ia^+, indicating that these stars have luminosities close to the Eddington limit[1].

In addition to these purely temperature and luminosity-class based categories, evolved massive stars are also found in some evolutionary transition phases, typically associated with strong mass-loss and eruptions. These classes are briefly introduced.

Wolf-Rayet Stars Stars with a Wolf-Rayet (WR) classification are of spectral-type O and comprise the hottest ($30\,000 - 200\,000$ K) sample of evolved massive stars. WR stars have strong stellar winds with high mass-loss rates ($10^{-5} - 10^{-4} M_\odot \mathrm{yr}^{-1}$) and wind velocities ranging from $\sim 1000\,\mathrm{km\,s^{-1}}$ up to $5500\,\mathrm{km\,s^{-1}}$. These intense winds peel off the outer shells of the star, uncovering successively the products from the various burning phases. The characteristic emission lines of WR stars are formed in the extended and dense high-velocity wind region enveloping the very hot stellar photosphere. According to the spectral appearance one distinguishes nitrogen-rich and carbon-rich WR stars as type WN (strong nitrogen lines) and WC (with carbon lines), or WO (with strong oxygen and carbon lines). WN and WC stars are further subdivided into early (E) and late (L) types: WNE (early WN, spreading from WN1 to WN5), respectively WCE (WC1 to WC5), and WNL (late WN, spreading from WN6 to WN11), respectively WCL (WC6 to WC9).

WR stars are descendants of massive main-sequence stars (with initial masses $> 25\,\mathrm{M}_\odot$) and most likely progenitors of core-collapse supernovae. More details on WR stars[2] and their physical properties can be found in Crowther (2007).

B[e] Supergiants A special class of blue supergiants comprise the B[e] supergiants. These are mostly supergiants of spectral type B (including a few objects of spectral types late-O and early-A) that are surrounded by dense circumstellar environments, typically in the form of a dusty disk and a massive, ionized polar wind. The central stars have luminosities in the range $10^4 < L/L_\odot < 10^6$.

---

[1]This is the maximum luminosity a star reaches when the outwards acting radiation force balances the inwards acting gravitational force.

[2]For a list with all Galactic WR stars see http://pacrowther.staff.shef.ac.uk/WRcat/

The circumstellar matter gives rise to numerous emission (e) lines, including emission from forbidden transitions (marked by square brackets), leading to the designation B[e]. Their massive disks are factories for various molecular species whose emission features allow to deduce the structure and kinematics of these disks (e.g., Kraus et al., 2015b; Maravelias et al., 2018), which might be highly dynamical and variable (Oksala et al., 2012; Torres et al., 2018) or long-lived enough to provide an environment suitable for the formation of even minor bodies or planets (Kraus et al., 2016).

B[e] supergiants are rare. They constitute just a few percent of all B-type supergiants. To date, a total of 33 objects has been identified and confirmed within the Milky Way and close-by galaxies, whereas another 25 objects have the status of B[e] supergiant candidates (Kraus, 2019).

Luminous Blue Variables Luminous Blue Variables (LBVs) are hot and luminous ($\log L/L_{\odot} > 5.4$) evolved massive stars that display characteristic variability in the form of either giant eruptions (such as the proto-type η Car) or excursions to the cool A-F-type supergiant region within the HR diagram in the form of an S Dor cycle named after the first object, S Dor in the Large Magellanic Cloud, showing this behavior. These excursions to the red are sometimes also termed 'outburst', but are not real outbursts connected with mass ejections but rather with an inflation of their envelopes at more or less constant luminosity.

S Dor cycles are a characteristic feature of LBVs based on which they can be distinguished from other types of hot luminous objects. They can last from years to decades. Without having displayed at least one full S Dor cycle or a major eruption, stars with otherwise similar properties to those of bona-fide LBVs, are only assigned the status of LBV candidates. A list of currently confirmed and candidate LBVs in Local Group galaxies is provided in Weis & Bomans (2020).

During the quiescent state of such an S Dor cycle, the stars appear like normal OB supergiants, sometimes displaying a WR-type (e.g., Maryeva et al., 2019) or a B[e] supergiant spectrum with intense emission lines. But from the latter they can be separated based on specific optical and infrared characteristics defined in Kraus (2019). Quiescent LBVs cluster along a diagonal region in the HR diagram called the LBV or S Dor instability strip (see Figure 1). When they reach maximum brightness in the S Dor cycle, they all appear at about the same cool temperature.

Due to the high mass-loss of LBVs and their (at least for some objects) giant eruptions, many LBVs are surrounded by nebulae of gas and dust with sizes of a few parsecs. While the morphology of the nebulae can be diverse, the majority displays bipolar structures (Weis, 2011).

It was long assumed that LBVs are a transitional phase in single star evolution. However, the detection of LBVs as progenitors of core-collapse supernovae is not in line with a transitional phase. Instead, it has been suggested that (at least some) LBVs might be the products of binary evolution (Smith, 2017).

Open Issues In summary, the evolution and final fate of massive stars depend severely on the initial conditions (mass, rotation speed, metallicity, magnetic fields, companion) and the amount of mass lost within each phase of their life.

Typically, stars within a certain category populate the same region within the HR diagram. However, diverse groups of stars may overlap, because they

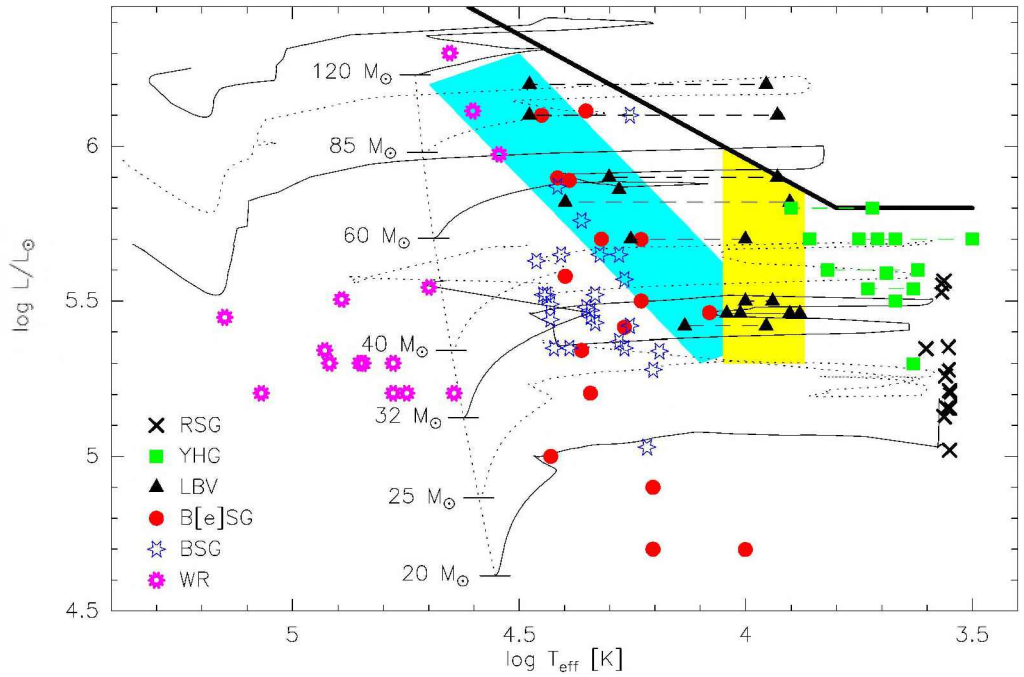

Figure 1. HR diagram for massive stars. Shown are evolutionary tracks of non-rotating stars from Ekström et al. (2012) for the indicated initial stellar masses on the ZAMS. Also included are representatives of the diverse groups of evolved massive stars. Dashes connecting symbols indicate the two temperature states, i.e., outburst and S Dor cycle for YHGs and LBVs, respectively. The thick solid kinked line represents the Humphreys-Davidson limit, the light-blue area marks the LBV/S Dor instability strip, and the yellow region highlights the Yellow Void.

have the same effective temperature and luminosity, but are in different evolutionary states (Figure 1). This can happen, because a certain combination of stellar parameters may occur more than once during the (red-ward, blue-ward, blue-loop) evolution of a massive star. Disentangling these populations is not always straight-forward. Consequently, some of the most relevant unsolved issues in massive star research comprise:

- What is their evolutionary state and connection to each other?
- Which physical mechanism causes enhanced mass-loss and outbursts?
- How much mass is lost and on which timescales?
- What is the structure and evolution of the ejected material?

Here, focus is given to the second item, and in the following observational and theoretical considerations of stellar pulsations in some types of evolved massive stars are discussed.

1.3. Pulsations in Evolved Massive Stars

Pulsations are nowadays ubiquitously found in stars all over the HR diagram. But currently, we cannot infer from observations whether massive stars in transition phases such as the LBVs, WRs and B[e]SGs are pulsating[3], because their dense winds usually hide their surfaces, and photometric variability is most likely affected by temporal changes in the wind and circumstellar matter rather than being purely due to pulsation activity. For the remaining of this Chapter, the attention is given to two groups of evolved massive stars: B supergiants and yellow hypergiants, and the possible role of pulsations as physical mechanism to trigger mass-loss and eruptions in these objects.

2. B Supergiants

Stars in the B supergiant (BSG) evolutionary state are the descendants of OB main-sequence stars. They have surface temperatures in the range $T_{\rm eff} = 10\,000 - 30\,000\,{\rm K}$ and luminosities of $L = 10^4 - 10^6\,L_\odot$. BSGs drive winds with mass-loss rates of $\dot{M} = 10^{-7} - 10^{-5}\,M_\odot{\rm yr}^{-1}$ and terminal velocities of $v_\infty = 200 - 3500\,{\rm km\,s}^{-1}$. These stars have been assumed to be well-behaved H-shell burning stars on their red-ward evolution, until the first BSG star exploded as supernova (SN1987A, West et al., 1987). While stars just off the main-sequence will not explode as supernova, this finding of a blue supergiant progenitor of SN1987A means that the group of BSGs consists of at least two coexisting populations: BSGs just beyond the main-sequence and BSGs in a post-red or post-yellow supergiant phase. A possible third population might comprise stars on a blue loop.

2.1. Characteristics of BSGs

BSGs can be characterized by three distinct properties, which are briefly outlined.

Light Curve Variability In principle, all OBA supergiants are variable in their visual light with amplitudes (A) and periods (P) of these microvariations in the range $A = 0.01 \ldots 0.1\,{\rm mag}$ and $P = 5 \ldots 100\,{\rm d}$, respectively. The variabilities have been reported to obey an amplitude-luminosity relation, meaning that the brightest stars display the largest amplitudes (Maeder & Rufener, 1972). The light variations follow no clear periodicities, instead they appear to be semi-regular. They are most pronounced in the sub-group of BA-type supergiants with luminosity class Ia. These extreme luminous stars are also often referred to as α Cygni variables (Sterken, 1977), named after the prototype of such stars α Cyg (Deneb). Detailed analyses of light curves of BSGs, e.g. from HIPPARCOS, resulted in the discovery of hundreds of new variable stars, of which 29 objects have been classified by Waelkens et al. (1998) as new α Cygni variables exhibiting clear periodic variations with amplitudes between 1 and a few tens of millimagnitude with periods ranging from a few hours to a few weeks.

[3]There is one exception: The B[e]SG star LHA 120-S 73 in the Large Magellanic Cloud has been suggested to pulsate based on detected line-profile variability of its photospheric He I line (Kraus et al., 2016).

Line-Profile Variability BSGs and their sub-class, the α Cyg variables, display variability in their line-profiles with Hα being the most prominent one. Due to the winds of the BSGs, their Hα lines display typically a P Cygni-type profile, which can vary significantly in strength and shape (see, e.g., Rosendhal, 1973; Kaufer et al., 1996). But also pure photospheric lines seem to display complex variability patterns indicating cyclic variations in radial velocities. This might indicate the possible simultaneous excitation of pulsation modes with periods typical for non-radial oscillations and radial overtones (Kaufer et al., 1997).

"Macro-turbulent" Line Broadening The most puzzling characteristic of BSGs is their huge amount of broadening in excess to stellar rotation. Simón-Díaz & Herrero (2007) analyzed photospheric line profiles of OB stars to derive the stellar rotation velocities projected to the line of sight ($v_{\rm rot} \sin i$) using the Fourier transform method. This mathematical approach is a very valuable tracer for stellar rotation velocities, because the Fourier transform of the rotation profile possesses zero points, which are correlated with $v_{\rm rot} \sin i$. Computing the Fourier transform of observed photospheric lines thus allows to directly read off the rotation velocity of the star projected to the line of sight. For more details on the stellar rotation profile and its Fourier transform, the interested reader is pointed to Chapter 18 in the textbook of Gray (2005).

The sample of Simón-Díaz & Herrero (2007) contained also OB supergiants, for which the authors recognized an extra, non-negligible broadening component. This component has more or less a Gaussian profile shape so that it has been dubbed as "macro-turbulence" without knowing a priori its physical origin. In fact, the velocities of this "macro-turbulence" needed to reproduce the observed widths of photospheric lines of BSGs turned out to exceed by far the value of the sound speed in the atmosphere of BSGs[4], meaning that this "macro-turbulence" has highly supersonic values (see Figure 1 in Simón-Díaz et al., 2010). If this velocity was due to real turbulences, shocks would form, creating X-ray emission which is not observed. Therefore, the extra broadening cannot be due to turbulence but must have another physical nature. And a possible explanation might be given by the superposition of many pulsations.

2.2. Discovery of Pulsations in BSGs

The previously mentioned characteristics of BSGs (light-curve and line-profile variability along with macro-turbulent line broadening) are a strong indication for a highly dynamical atmosphere and might point towards the presence of oscillations in these luminous objects. However, it was not expected that BSGs pulsate because of their radiative helium core, which immediately damps all modes propagating towards the core. Therefore, it was a big surprise when Saio et al. (2006) reported on the discovery of multiple oscillations in the BSG star HD 163899. These authors had analyzed a 37 day long continuous, high precision photometric light curve collected with the Canadian satellite MOST. Their studies revealed 48 periods from 10 h to 25 d, which they assigned to pulsations in both p-modes and g-modes.

[4]As an example, a value of $v_{\rm macro} = 80\,{\rm km\,s^{-1}}$ along with $v_{\rm rot} \sin i = 47\,{\rm km\,s^{-1}}$ is needed to fit the shape of the Si III lines of the B0 Ia supergiant star HD 89767, (see Figure 4 in Puls, 2008).

Especially the occurrence of g-modes in a post-main sequence massive supergiant star was surprising. The stability analysis of Saio et al. (2006) revealed that the existence of g-modes can be explained by the development of an intermediate convective zone (ICZ) connected with the hydrogen burning shell. This ICZ results from a semi-convection episode during the main-sequence evolution. At this convective zone selected g-modes can be reflected back towards the surface. The ICZ hence prevents the modes from penetrating the radiative damping core of the star and, therefore, supports the establishment of g-mode pulsations. But for this, the position of the ICZ within the envelope plays an important role. If it is located too close to the surface, oscillations cannot be excited, and if it is too close to the core, the excited oscillations will be significantly damped. Moreover, the presence of physical effects such as rotation (mixing) and magnetic fields, as well as the strength of mass-loss, semi-convection, and overshooting during the main-sequence evolution have been found to influence the evolution of massive stars and thus can favor or prevent the formation of the ICZ (see, e.g., Godart et al., 2009, 2014). In that respect it is worth mentioning that follow-up investigations of Daszyńska-Daszkiewicz et al. (2013) have shown that the detection of pulsations is not necessarily a proof for the existence of an ICZ, but only for the presence of *some* reflective layer, which might also have a different physical origin.

Saio et al. (2006) computed stellar models using the updated OPAL opacities (Iglesias & Rogers, 1996) for stars covering a range of initial masses of 7–20 $M_\odot$ from the main-sequence into the BSG domain. As in most stars, it is the κ-mechanism that excites the modes in BSGs. This mechanism acts due to the iron-opacity bump in the superficial layers. Their analysis revealed a new instability domain for g-mode pulsations, covering the loci of BSGs in the HR diagram. For the BSG star HD 163899 the frequencies of these pulsations were in fairly good agreement with the frequencies found from the photometric light curve. Follow-up studies of BSGs with known photometric variability, e.g. from HIPPARCOS light curves, were found to have stellar parameters that placed them into the newly identified instability domain and were hence considered as gravity-mode pulsators (Lefever et al., 2007).

With the knowledge of multiple g-mode pulsations acting in BSGs, Aerts et al. (2009) could show that the shapes of the metal line profiles of BSGs can be naturally explained by combining the broadening caused by the velocity of hundreds of low-amplitude, non-radial gravity-mode pulsations. This was the first firm proof that pulsations can significantly contribute to (if not completely explain) the "macro-turbulent" line broadening observed in BSGs. Besides g-mode pulsations as the cause for "macro-turbulence" other scenarios appeared in the literature and require further notice. One of them comprises stochastically excited oscillations caused by subsurface convection (Grassitelli et al., 2015), another one proposes convectively driven internal gravity waves (Aerts & Rogers, 2015). Which of them is really responsible for the "macro-turbulence" in BSGs needs to be further studied, and maybe the truth lies in the interplay of more than one effect.

2.3. Pulsation Behavior in the Different BSG Populations

The discovery of pulsations in BSGs and the identification of the new instability domain helped to explain the observed variabilities in a number of BSGs. However, those BSGs that were classified as α Cygni variables display variabilities that point towards multiple periods spreading over a large period range. These are not in agreement with what would be expected from pure non-radial g-mode oscillations. Especially the long periods are more likely connected to radial modes. To test this hypothesis, Saio et al. (2013) extended their calculations of pulsation instabilities and computed the pulsation patterns following the evolution of massive stars up to the red-supergiant (RSG) stage and beyond for stars with initial masses up to 25 $M_\odot$. They did that for the case of both non-rotating stars and stars rotating initially with 40% of their critical speed.

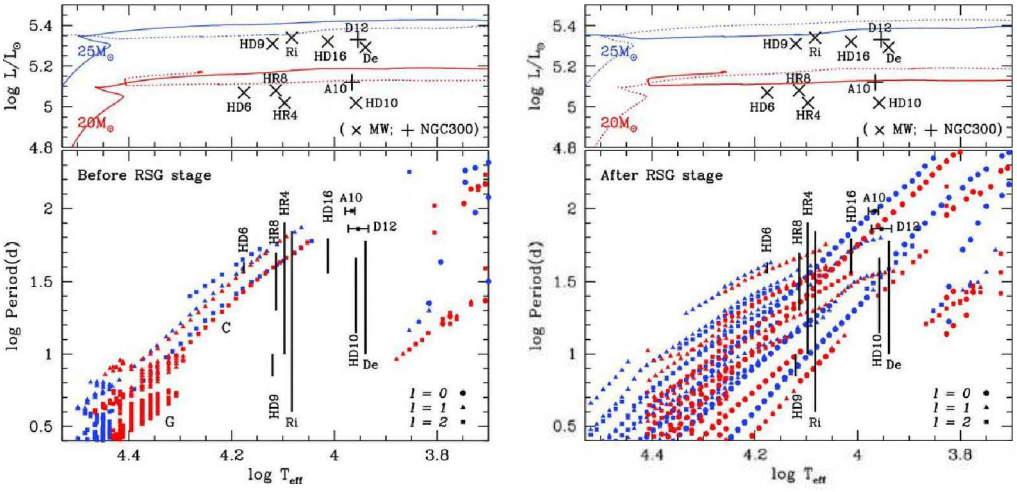

Figure 2. Evolutionary tracks (top) of stars with rotation and the excited pulsation periods in the models (bottom) during the pre- (left) and post-RSG (right) phase. For comparison, the period ranges of some α Cyg variables in the Milky Way and NGC 300 are included. Figure is taken from Saio et al. (2013) (their Figure 5).

As stellar evolution calculations of Ekström et al. (2012) have shown, rotating stars tend to evolve back to the blue side of the HR diagram after having passed through a cool, RSG phase, whereas non-rotating stars evolve only to the RSG stage and explode there as supernovae. Based on these latter models, the calculations of Saio et al. (2013) (see Figure 2) predict the excitation of radial pulsations only during the main-sequence and shortly after, and during their RSG state. In between, i.e. in the temperature regime from 20 000 K down to about 6 000 K where the α Cygni variables reside, no radial modes are excited.

For the stellar models with rotation, the situation with respect to the excitation of radial modes during the pre-RSG evolution is very similar to the non-rotating models, and the radial fundamental mode is only excited within the β Cephei instability region. Within the BSG domain only very few oscillatory convection modes are predicted which cannot explain the number and period

range of the observed oscillations in α Cygni variables. However, after the stars have passed through the RSG state, they develop a complex frequency behavior. They are capable to establish and maintain numerous pulsation modes spreading over a large period range, in agreement with the range of observed periods in the α Cygni variables.

Among the excited modes are several radial ones, including the so-called radial strange modes. These strange modes are particularly interesting, because they have been proposed to cause pulsation-driven time-variable mass-loss (Glatzel et al., 1999), leading to the interpretation of periodic variability of supergiants in terms of strange-mode instabilities (Glatzel & Kiriakidis, 1993). A prerequisite for their excitation is that the star needs to reach a luminosity over mass ratio of $L_*/M_* > 10^4\,\mathrm{L}_\odot/\mathrm{M}_\odot$ (Gautschy & Glatzel, 1990; Glatzel, 1994). Exceeding such a limit is no problem for massive stars that have passed through the RSG phase, during which they tend to loose a significant fraction of their mass via dense dust-driven winds thus increasing their L_*/M_* easily by a factor of 2 or more. Consequently, post-RSGs have much lower masses but similar luminosities than their younger pre-RSG counterparts, and present a completely different pulsation behavior. These differences can be used to pin down the evolutionary stage of BSGs by sorting them into pre- and post-RSGs, and to identify in such way possible supernova progenitors, for which the α Cygni variables seem to be suitable candidates.

2.4. Identification of Pulsations in BSGs

For the identification of stellar pulsations two types of observations are typically used: photometric light curves and spectroscopic time series.

Photometric Light Curves Photometric variability in BSGs has been detected based on light curves, especially from satellite missions such as HIPPARCOS and MOST as mentioned before. But also other satellites such as BRITE and TESS observed (and still observe) a number of them.

However, light curves of BSGs, especially when the band passes are optimized for the red, face two issues. Firstly, BSGs have stellar winds, which is obvious from P Cygni-type profiles of their Hα lines. These winds are not steady but vary in time as can be seen from the sample of Hα profile shapes of the BSG star 55 Cyg shown in Figure 3. But the variation is not periodic, as has been demonstrated by Kraus et al. (2015a). The wavelength range covering Hα is contained in the white-light filter of HIPPARCOS, and in both the red band pass of BRITE and the wide band pass of TESS. Therefore, any variability in the Hα line due to changes in the wind conditions will automatically imprint a variability signature on the stellar brightness measured by the photometric magnitude.

Second, depending on their density distribution, the winds of BSGs can alter the continuum flux. These winds have a radial velocity distribution that is usually described with the so-called β-law, defined by $v(r) = v_0 + (v_\infty - v_0)(1 - R_*/r)^\beta$, where v_∞ is the terminal wind velocity, v_0 is the velocity at the base of the wind, R_* is the stellar radius, and β describes the "steepness" of the velocity increase. Values of β for OB stars with line-driven winds are normally in the range 0.8-1.0, but for many BSGs, β has been proposed to take values of 3 or

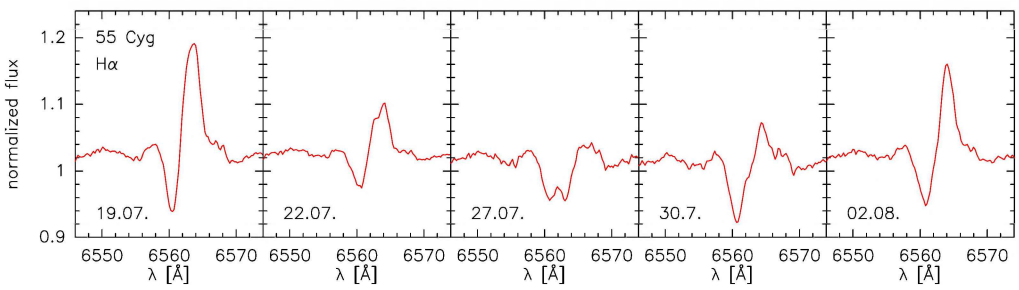

Figure 3. Snapshots of the Hα line of the BSG star 55 Cyg demonstrating the wind variability. The data were taken during a 14-day period in 2013 with the Perek 2-m telescope at Ondřejov Observatory.

even higher (e.g., Crowther et al., 2006). However, the higher the value of β, the higher is the density within the innermost wind region. As has been shown by Kraus et al. (2008), winds of BSGs with $\beta > 1$ significantly contribute with their free-free and free-bound emission to the total continuum emission, especially in the red part of the spectrum. Any variation in the wind thus produces an additional variability signal that influences and perturbs the measured stellar brightness and can (maybe severely) hamper the frequency analysis.

Considering these two effects, it is questionable whether photometric observations in broad-band filters or even in white light (such as TESS) can provide reliable insight into the pulsation behavior of those BSGs (such as the α Cygni variables), whose photometric fluxes are contaminated by variable wind emission due to significant changes in stellar mass-loss rates affecting both the red continuum and the Hα line profile.

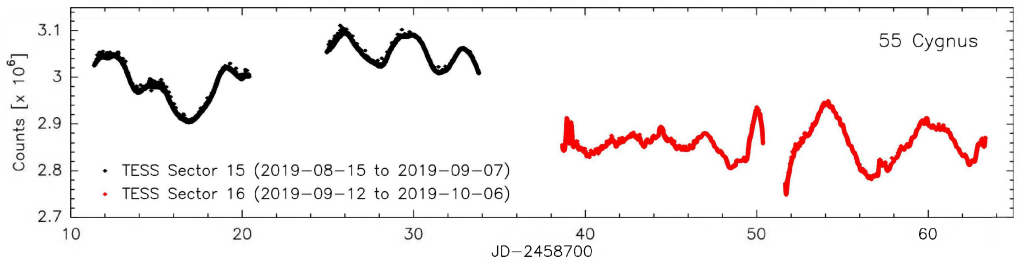

Figure 4. TESS example light curve of the α Cygni variable 55 Cygnus.

An example of a TESS light curve[5] of an α Cyg variable is shown in Figure 4. TESS has observed this star during two periods labeled as sectors 15 and 16. Obviously, the character of the variability has changed between the two observing runs. While it showed a smooth behavior during the first period, it appears more irregular and chaotic during the second one.

[5]The data described here may be obtained from the MAST archive at https://dx.doi.org/10.17909/t9-ncv5-bb52.

Spectroscopic Time Series Spectroscopic time series of high-quality (in both resolution and signal-to-noise level) provide an excellent tool to unveil whether the variability in the observed line profiles are due to pulsations, and to investigate whether the periodicities are strict such as for long-term coherent modes. This requires the monitoring of photospheric lines, typically of metals, which are not affected by superimposed emission from the stellar wind.

As has been discussed in a previous Chapter, pulsations cause changes in radial velocity and in the profile shape of the lines. To quantify these parameters, we make use of the so-called "velocity moments" of the lines, based on which a line profile is fully characterized (see, e.g., Aerts et al., 1992, 2010a; North & Paltani, 1994). Considering that a spectral line is a set of discrete measurements (λ_i, F_i), its moments are defined in the following way:

$$M_0 = \sum_{i=1}^{N}(1-F_i)\Delta x_i, \quad (1)$$

$$M_1 = \sum_{i=1}^{N}(1-F_i)(x_i-x_0)\Delta x_i, \quad (2)$$

$$M_2 = \sum_{i=1}^{N}(1-F_i)(x_i-x_0)^2\Delta x_i, \quad (3)$$

$$M_3 = \sum_{i=1}^{N}(1-F_i)(x_i-x_0)^3\Delta x_i, \quad (4)$$

with the normalized flux F_i measured at wavelength λ_i for pixel i, $\Delta x_i = x_i - x_{i-1}$ whereby x_i is the velocity corresponding to λ_i with respect to the laboratory wavelength of the line (λ_0), and x_0 is the relative motion of the star with respect to the Sun that needs to be corrected for to guarantee that the odd moments have an average of zero.

For practical purposes one utilizes the normalized moments, which are defined as $\langle v^j \rangle = M_j/M_0$ for $j = 1, 2, 3$. The units of these moments are $(\mathrm{km\,s^{-1}})^j$, and the first three of these normalized moments are connected to specific properties of the profile:

$\langle v^1 \rangle$ is the radial velocity, i.e., a measure for the center of gravity of the line,

$\langle v^2 \rangle$ provides a measure for the line width, and

$\langle v^3 \rangle$ measures the skewness, i.e. the asymmetry of the profile.

Each photospheric line forms over a certain range of depth in the atmosphere, and the actual velocity of motion is a function of stellar longitude, latitude, and depth. Moreover, we see the stellar surface only in its projection, and the radial velocity is inferred from the integration over that projected surface. Therefore, the first moment provides not any pulsation velocity, but it can be used to derive the periods of the pulsations.

The variations recorded in the moments can furthermore be used to separate pulsating stars from stars with other types of variability, such as stars with surface spots. Stellar spots are commonly seen in chemically peculiar stars, in which localized over- and under-abundances in specific elements cause surface inhomogeneities. Consequently, the variability in such stars is linked to the stellar rotation period, and different elements display diverse variabilities (see e.g., Briquet et al., 2004; Lehmann et al., 2006) in contrast to pulsating stars, in which the lines from different elements vary in phase. Moreover, theoretically generated profiles of pulsating stars have revealed that their first and third normalized moments vary in phase as well (de Pauw et al., 1993). This property is also useful to discriminate pulsating stars from objects with spots (e.g., Briquet et al., 2004).

Application of the moment method to spectroscopic time series of two BSG stars (σ Cyg and 55 Cyg) collected with the Perek 2-m telescope in the wavelength range $6250 - 6750$ Å with a spectral resolution of 13 000 and a signal-to-noise ratio of $S/N > 300$ resulted in interesting discoveries. For σ Cyg, a very short oscillation period of just 1.59 hours (Kraus et al., 2012) has been identified from several short-term time series of the photospheric Si II and He I lines (Figure 5).

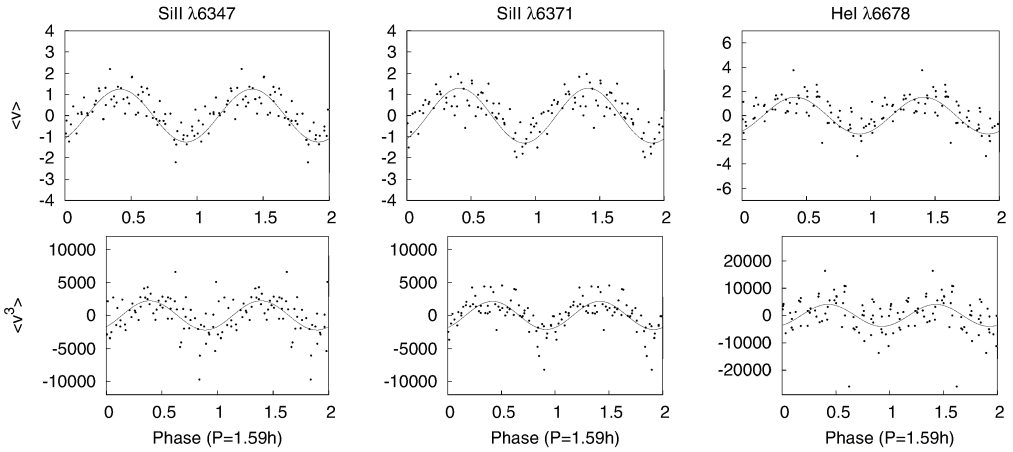

Figure 5. First and third moment of the photospheric Si II $\lambda\lambda$6347,6371 and the He I λ6678 lines of the BSG star σ Cyg. The spectroscopic time series were taken in 2010 and 2012. The oscillation character is deduced from the fact that both, the first and third moments of each element and the moments of different elements vary in phase. The data have been phased to the identified period of 1.59 h. Credit: Kraus et al. (2012), reproduced with permission ©ESO.

In the long-term spectroscopic time series of the BSG star 55 Cyg, a total of 19 periods have been found from the analysis of the radial velocity curve of the photospheric He I λ6678 line. These periods range from a few hours to 22.5 days, in agreement with their classification as p-modes, g-modes, and at least one radial strange mode (Kraus et al., 2015a). Moreover, the analysis of the

wind and stellar parameters of 55 Cyg based on computation of the Balmer, helium and silicon lines using the FASTWIND code (Puls et al., 2005) revealed that the star has a time-variable radius along with variable wind conditions, in agreement with cyclic phases of enhanced mass-loss. In particular, for the stellar parameters it has been found that the effective temperature, $T_{\rm eff}$, ranges from 18 570 K to 19 100 K, the stellar radius is $R_* = 57 \pm 1\,{\rm R}_\odot$ but varies from 52 to 65 $\rm R_\odot$, and the stellar luminosity is $\log L_*/L_\odot = 5.57 \pm 0.03$. With a spectroscopic mass of $34 \pm 4\,M_\odot$, $L_*/M_* > 10^4\,L_\odot/M_\odot$, which is the needed condition for the star to be able to excite strange mode pulsations. In addition, the line profiles revealed values for $v_{\rm rot} \sin i = 50 - 60\,{\rm km\,s^{-1}}$ and $v_{\rm macro} = 10 - 50\,{\rm km\,s^{-1}}$.

For the wind parameters of 55 Cyg it was found that $\dot{M}$ varies between 1.5×10^{-7} and $4.6 \times 10^{-7} M_\odot {\rm yr}^{-1}$, meaning that the change in mass loss occasionally exceeds a factor of 3. In addition, v_∞ varies between 230 and 350 $\rm km\,s^{-1}$, with exceptions of 600 and 700 $\rm km\,s^{-1}$ at times when also the mass-loss rates were increased. The large amount of detected periods including a radial strange mode resulted in the classification of 55 Cyg as a post-RSG object and hence as an α Cyg variable.

The findings of multiple pulsation periods in 55 Cyg have been confirmed by numerical non-linear simulations performed by Yadav & Glatzel (2016). Their calculations additionally unveiled that 55 Cyg undergoes strange-mode instabilities with triggered mass-loss, in agreement with the results derived from the observations.

Periodic mass-loss episodes related to a time-variable oscillation mode have also been found in the BSG star HD 50064 (Aerts et al., 2010b), and wind variability along with a pulsation–mass-loss relation was postulated for a sample of BSGs by Haucke et al. (2018). These results reinforce the need of in depth studies of the pulsation and mass-loss properties and their interrelation in these luminous objects.

3. Yellow Hypergiants

Stars falling into the category of yellow hypergiants (YHGs) reside in the temperature regime $T_{\rm eff} = 4000 - 9000\,{\rm K}$ and have luminosities of $L = 10^{5.3} - 10^{5.8}\,L_\odot$. These objects have evolved from progenitor stars with initial masses in the range $25 - 50\,M_\odot$. YHGs are rare objects, implying a short lifetime of this evolutionary transition phase. In total we currently know of ~30 objects that are classified as YHGs or YHG candidates in the Milky Way and neighboring galaxies of the Local Group (e.g., de Jager, 1998; Clark et al., 2005; Kourniotis et al., 2017), and so far, only a handful of them have been thoroughly examined.

YHGs have been proposed to have passed through the RSG phase and evolve now back to the hot side of the HR diagram (de Jager, 1998). The structure of YHGs can best be approximated by a compact core that is surrounded by a huge inflated, low-density envelope. Due to this inflation, the surface gravity of YHGs is very small or can even approach a value of zero. This means, that even smallest perturbations within the atmosphere can initiate mass-loss from the star.

When the star reaches a surface temperature of $\sim$ 7000 K, its atmosphere becomes dynamically unstable (Nieuwenhuijzen & de Jager, 1995; Lobel, 2001).

Strong mass loss sets in, creating what is called a pseudo-photosphere and veiling the central object. Such an outburst phase can last from a few months up to years during which the pseudo-photosphere mimics a much cooler temperature of the object. Only after the termination of the strongly enhanced mass-loss and when the released material has diluted, the star appears back at its real (hotter) temperature. This process repeats until the stellar atmosphere finally reaches again an equilibrium state. However, for a stable state, the star must reach an effective temperature of about 12000 K. This means that the star remains unstable until it has lost its complete outer layers, which is done most likely in a series of such outbursts. The temperature region of this instability domain, spreading from 7000 to 12000 K in the HR diagram, appears to be vacant of stars and was thus called the Yellow Void.

Because the star seems to move back and forwards in the HR diagram, YHGs are indicated in Figure 1 by connecting lines between the real (hot) position of the star and its position during outburst (cool). The multiple attempts of the star to pass through this temperature domain has been described as bouncing at the Yellow Void (de Jager, 1998) respectively Yellow Wall (Oudmaijer et al., 2009). As a consequence of this bouncing and the multiple mass ejection phases, the star might be surrounded by several distinct shells of gas and dust as is seen, e.g., around the star IRAS 17163-3907 dubbed as the fried-egg nebula (Lagadec et al., 2011).

Most famous for its outbursts is the Galactic YHG star ρ Cas (=HD 224014). This star has been monitored for more than a century. During that time, the star underwent several outbursts with major events in 1945–1947, 1985–1986, 2000–2001, and a most recent, shorter and less pronounced one in 2013 (Kraus et al., 2019). The outbursts can be traced by a strong decrease in brightness by more than 1 mag in V-band along with the development of spectroscopic signatures of molecules such as TiO and CO that form within the developing cool, massive wind (e.g., Lobel et al., 2003; Gorlova et al., 2006). The decrease in the time interval between individual outbursts might indicate that the star could be preparing for a major eruption that might help to catapult it out of the Yellow Void instability region and would finally allow the star to reach a new, hot equilibrium state.

In contrast to ρ Cas, the YHG star V509 Cas (=HD 217476, HR 8752) displayed a different behavior over the past $\sim$ 150 yr. It also underwent a number of material ejection events during which a pseudo-photosphere was produced and the temperature dropped. However, underneath these temperature fluctuations the star experienced a real increase in effective temperature from about 5000 K back in 1973 to 8000 K in 2001 (Nieuwenhuijzen et al., 2012). Since then, this development seems to have stopped (Aret et al., 2017). A similar trend with an increasing effective temperature has been reported for the YHG object IRC+10420. Spectroscopic monitoring of this object revealed that it has changed from spectral type F8 to a mid-A type, meaning that it heated up by more than 1000 K over the course of about 20 years (Oudmaijer et al., 1996; Oudmaijer, 1998), and then stabilized in the vicinity of the high-temperature boundary of the Yellow Void (Klochkova et al., 2016).

3.1. Indications for Pulsations in YHGs

Outside their outburst phases YHGs display both spectroscopic and photometric variability, that are reminiscent of pulsation activity.

Theoretical investigations by Fadeyev (2011) proposed that the κ-mechanism operating in the helium ionization zones can cause radial pulsations with periods up to 200 d. However, the observed light curves of YHGs display low-amplitude photometric variability which has quasi-periods that are much longer, reaching a few hundred days (e.g., Percy & Zsoldos, 1992; Arkhipova et al., 2009; Kraus et al., 2019). These quasi-periods can most likely be ascribed to semi-regular, non-radial pulsations (Lobel et al., 1994).

Spectroscopic monitoring reveals that the atmospheres of YHGs are highly dynamical, as has been proven by radial velocity measurements of a variety of atmospheric lines formed in different depths (e.g., Klochkova et al., 2014; Klochkova, 2019). These atmospheric motions also display a quasi-periodic variation in agreement with semi-regular pulsations, and it has been found that this pulsation activity increases, i.e. develops larger velocity amplitudes prior to outbursts (Lobel et al., 2003; Kraus et al., 2019). Such a behavior is commonly observed in relation to the excitation and development of strange mode instabilities. Alike the α Cygni variables YHGs have lost a significant amount of mass during their previous RSG evolution so that they fulfill the required criteria of a high luminosity to mass ratio for strange mode excitation, and detailed numerical investigations are badly needed and currently underway that will help to deepen our comprehension of pulsations in YHGs and their ability to trigger outbursts.

4. Conclusions

This Chapter was devoted to some intriguing post-main sequence phases through which a massive star may evolve and which have been reported to display pulsations. Among them were the BSGs, which can be either in a pre- or a post-RSG stage, the latter are also known as α Cygni variables. It has been shown that these two populations display divers pulsation properties. In particular, stars in the post-RSG phase typically display many more pulsation modes than their younger counterparts. Detailed pulsation analyses of BSGs can thus provide a meaningful tool to separate these two BSG populations. However, care should be taken with the choice of data for the analysis. The photometric light curves might be contaminated by the variable emission of their high-density winds, which can lead to false results.

A second group of objects, that has been presented, are comprised by the YHGs. Alike the α Cygni variables, YHGs are also massive stars in their post-RSG evolution, but these objects reside still within the cool, yellow domain of the HR diagram. YHGs perform long-term (several hundred days) quasi-periodic oscillations and undergo from time to time outbursts with strongly enhanced mass loss. These outbursts, which are also related to the formation of a pseudo-photosphere, lead to an apparent (much) cooler temperature of the object. Moreover, the objects display a strongly enhanced pulsation activity prior to the outbursts.

Both groups of stars, the α Cygni variables and the YHGs, provide ideal conditions for the excitation of strange-mode instabilities. Investigations of the properties of such strange modes revealed that these instabilities can lead to significant mass-loss, which can reach values comparable to or even in excess to those from the line-driven winds of these objects. Consequently, strange-mode pulsations might provide an important component to the observed wind variability and the formation of structures and density inhomogeneities in the winds of α Cygni variables. Moreover, they might be a suitable trigger for the outbursts observed in YHGs.

YHGs and α Cygni variables are cornerstone objects in the evolution of massive stars, because they constitute a link between the cool RSGs and the hot pre-supernova evolutionary stages such as Wolf-Rayet stars and Luminous Blue Variables. Detailed knowledge about the mass-loss behavior in these transition phases in stellar evolution is essential because the mass loss controls the fate of these fascinating objects.

Acknowledgments. I wish to thank the SOC and LOC for their fantastic job in organizing and implementing this interesting and pleasant Summer School. This paper includes data collected with the TESS mission, obtained from the MAST data archive at the Space Telescope Science Institute (STScI). Funding for the TESS mission is provided by the NASA Explorer Program. STScI is operated by the Association of Universities for Research in Astronomy, Inc., under NASA contract NAS 5-26555. The Astronomical Institute, Czech Academy of Sciences, is supported by the project RVO:67985815. This project has received funding from the Czech Science Foundation (GA ČR 20-00150S) and from the European Union's Framework Programme for Research and Innovation Horizon 2020 (2014-2020) under the Marie Skłodowska-Curie Grant Agreement No. 823734.

References

Aerts C., Christensen-Dalsgaard J., Kurtz D. W., 2010a, *Asteroseismology*

Aerts C., de Pauw M., Waelkens C., 1992, *A&A*, **266**, 294

Aerts C., Lefever K., Baglin A., Degroote P., Oreiro R., Vučković M., Smolders K., Acke B., Verhoelst T., Desmet M., Godart M., Noels A., Dupret M. A., Auvergne M., Baudin F., Catala C., Michel E., Samadi R., 2010b, *A&A*, **513**, L11

Aerts C., Puls J., Godart M., Dupret M. A., 2009, *A&A*, **508(1)**, 409

Aerts C., Rogers T. M., 2015, *ApJL*, **806(2)**, L33

Aret A., Kolka I., Kraus M., Maravelias G., 2017, A. Miroshnichenko, S. Zharikov, D. Korčáková, and M. Wolf (eds.), *The B[e] Phenomenon: Forty Years of Studies*, Vol. 508 of *Astronomical Society of the Pacific Conference Series*, p. 239

Arkhipova V. P., Esipov V. F., Ikonnikova N. P., Komissarova G. V., Tatarnikov A. M., Yudin B. F., 2009, *Astronomy Letters*, **35(11)**, 764

Briquet M., Aerts C., Lüftinger T., De Cat P., Piskunov N. E., Scuflaire R., 2004, *A&A*, **413**, 273

Castor J. I., Abbott D. C., Klein R. I., 1975, *ApJ*, **195**, 157

Clark J. S., Negueruela I., Crowther P. A., Goodwin S. P., 2005, *A&A*, **434(3)**, 949

Crowther P. A., 2007, *ARA&A*, **45(1)**, 177
Crowther P. A., Lennon D. J., Walborn N. R., 2006, *A&A*, **446(1)**, 279
Curé M., 2004, *ApJ*, **614(2)**, 929
Daszyńska-Daszkiewicz J., Ostrowski J., Pamyatnykh A. A., 2013, *MNRAS*, **432(4)**, 3153
de Jager C., 1998, *A&A Rev.*, **8(3)**, 145
de Pauw M., Aerts C., Waelkens C., 1993, *A&A*, **280(2)**, 493
Dufton P. L., Langer N., Dunstall P. R., Evans C. J., Brott I., de Mink S. E., Howarth I. D., Kennedy M., McEvoy C., Potter A. T., Ramírez-Agudelo O. H., Sana H., Simón-Díaz S., Taylor W., Vink J. S., 2013, *A&A*, **550**, A109
Ekström S., Georgy C., Eggenberger P., Meynet G., Mowlavi N., Wyttenbach A., Granada A., Decressin T., Hirschi R., Frischknecht U., Charbonnel C., Maeder A., 2012, *A&A*, **537**, A146
Fadeyev Y. A., 2011, *Astronomy Letters*, **37(6)**, 403
Gautschy A., Glatzel W., 1990, *MNRAS*, **245**, 597
Glatzel W., 1994, *MNRAS*, **271**, 66
Glatzel W., Kiriakidis M., 1993, *MNRAS*, **263**, 375
Glatzel W., Kiriakidis M., Chernigovskij S., Fricke K. J., 1999, *MNRAS*, **303(1)**, 116
Godart M., Grotsch-Noels A., Dupret M.-A., 2014, J. A. Guzik, W. J. Chaplin, G. Handler, and A. Pigulski (eds.), *Precision Asteroseismology*, Vol. 301 of *IAU Symposium*, pp 313–320
Godart M., Noels A., Dupret M. A., Lebreton Y., 2009, *MNRAS*, **396(4)**, 1833
Gorlova N., Lobel A., Burgasser A. J., Rieke G. H., Ilyin I., Stauffer J. R., 2006, *ApJ*, **651(2)**, 1130
Grassitelli L., Fossati L., Simón-Diáz S., Langer N., Castro N., Sanyal D., 2015, *ApJL*, **808(1)**, L31
Gray D. F., 2005, *The Observation and Analysis of Stellar Photospheres*
Haucke M., Cidale L. S., Venero R. O. J., Curé M., Kraus M., Kanaan S., Arcos C., 2018, *A&A*, **614**, A91
Iglesias C. A., Rogers F. J., 1996, *ApJ*, **464**, 943
Kaufer A., Stahl O., Wolf B., Fullerton A. W., Gaeng T., Gummersbach C. A., Jankovics I., Kovacs J., Mandel H., Peitz J., Rivinius T., Szeifert T., 1997, *A&A*, **320**, 273
Kaufer A., Stahl O., Wolf B., Gaeng T., Gummersbach C. A., Kovacs J., Mandel H., Szeifert T., 1996, *A&A*, **305**, 887
Klochkova V. G., 2019, *Astrophysical Bulletin*, **74(4)**, 475
Klochkova V. G., Chentsov E. L., Miroshnichenko A. S., Panchuk V. E., Yushkin M. V., 2016, *MNRAS*, **459(4)**, 4183
Klochkova V. G., Panchuk V. E., Tavolzhanskaya N. S., Usenko I. A., 2014, *Astronomy Reports*, **58(2)**, 101
Kourniotis M., Bonanos A. Z., Yuan W., Macri L. M., Garcia-Alvarez D., Lee C. H., 2017, *A&A*, **601**, A76
Kraus M., 2006, *A&A*, **456(1)**, 151
Kraus M., 2019, *Galaxies*, **7(4)**, 83
Kraus M., Cidale L. S., Arias M. L., Maravelias G., Nickeler D. H., Torres A. F., Borges Fernandes M., Aret A., Curé M., Vallverdú R., Barbá R. H., 2016, *A&A*, **593**, A112

Kraus M., Haucke M., Cidale L. S., Venero R. O. J., Nickeler D. H., Németh P., Niemczura E., Tomić S., Aret A., Kubát J., Kubátová B., Oksala M. E., Curé M., Kamiński K., Dimitrov W., Fagas M., Polińska M., 2015a, *A&A*, **581**, A75

Kraus M., Kolka I., Aret A., Nickeler D. H., Maravelias G., Eenmäe T., Lobel A., Klochkova V. G., 2019, *MNRAS*, **483(3)**, 3792

Kraus M., Kubát J., Krtička J., 2008, *A&A*, **481(2)**, 499

Kraus M., Oksala M. E., Cidale L. S., Arias M. L., Torres A. F., Borges Fernandes M., 2015b, *ApJL*, **800(2)**, L20

Kraus M., Tomić S., Oksala M. E., Smole M., 2012, *A&A*, **542**, L32

Lagadec E., Zijlstra A. A., Oudmaijer R. D., Verhoelst T., Cox N. L. J., Szczerba R., Mékarnia D., van Winckel H., 2011, *A&A*, **534**, L10

Lamers H. J. G. L. M., Cassinelli J. P., 1999, *Introduction to Stellar Winds*

Lefever K., Puls J., Aerts C., 2007, *A&A*, **463(3)**, 1093

Lehmann H., Tsymbal V., Mkrtichian D. E., Fraga L., 2006, *A&A*, **457(3)**, 1033

Lobel A., 2001, *ApJ*, **558(2)**, 780

Lobel A., de Jager C., Nieuwenhuijzen H., Smolinski J., Gesicki K., 1994, *A&A*, **291**, 226

Lobel A., Dupree A. K., Stefanik R. P., Torres G., Israelian G., Morrison N., de Jager C., Nieuwenhuijzen H., Ilyin I., Musaev F., 2003, *ApJ*, **583(2)**, 923

Maeder A., 2009, *Physics, Formation and Evolution of Rotating Stars*

Maeder A., Rufener F., 1972, *A&A*, **20**, 437

Maravelias G., Kraus M., Cidale L. S., Borges Fernand es M., Arias M. L., Curé M., Vasilopoulos G., 2018, *MNRAS*, **480(1)**, 320

Martins F., Palacios A., 2013, *A&A*, **560**, A16

Maryeva O., Viotti R. F., Koenigsberger G., Calabresi M., Rossi C., Gualandi R., 2019, *Galaxies*, **7(3)**, 79

Meynet G., Maeder A., 2000, *A&A*, **361**, 101

Nieuwenhuijzen H., de Jager C., 1995, *A&A*, **302**, 811

Nieuwenhuijzen H., De Jager C., Kolka I., Israelian G., Lobel A., Zsoldos E., Maeder A., Meynet G., 2012, *A&A*, **546**, A105

North P., Paltani S., 1994, *A&A*, **288**, 155

Oksala M. E., Kraus M., Arias M. L., Borges Fernand es M., Cidale L., Muratore M. F., Curé M., 2012, *MNRAS*, **426(1)**, L56

Oudmaijer R. D., 1998, *A&AS*, **129**, 541

Oudmaijer R. D., Davies B., de Wit W. J., Patel M., 2009, *Post-Red Supergiants*, Vol. 412 of *Astronomical Society of the Pacific Conference Series*, p. 17

Oudmaijer R. D., Groenewegen M. A. T., Matthews H. E., Blommaert J. A. D. L., Sahu K. C., 1996, *MNRAS*, **280(4)**, 1062

Pelupessy I., Lamers H. J. G. L. M., Vink J. S., 2000, *A&A*, **359**, 695

Percy J. R., Zsoldos E., 1992, *A&A*, **263**, 123

Puls J., 2008, F. Bresolin, P. A. Crowther, and J. Puls (eds.), *Massive Stars as Cosmic Engines*, Vol. 250 of *IAU Symposium*, pp 25–38

Puls J., Urbaneja M. A., Venero R., Repolust T., Springmann U., Jokuthy A., Mokiem M. R., 2005, *A&A*, **435(2)**, 669

Ramírez-Agudelo O. H., Simón-Díaz S., Sana H., de Koter A., Sabín-Sanjulían C., de Mink S. E., Dufton P. L., Gräfener G., Evans C. J., Herrero A., Langer N., Lennon D. J., Maíz Apellániz J., Markova N., Najarro F., Puls J., Taylor W. D., Vink J. S., 2013, *A&A*, **560**, A29

Rosendhal J. D., 1973, *ApJ*, **182**, 523
Saio H., Georgy C., Meynet G., 2013, *MNRAS*, **433(2)**, 1246
Saio H., Kuschnig R., Gautschy A., Cameron C., Walker G. A. H., Matthews J. M., Guenther D. B., Moffat A. F. J., Rucinski S. M., Sasselov D., Weiss W. W., 2006, *ApJ*, **650(2)**, 1111
Simón-Díaz S., Herrero A., 2007, *A&A*, **468(3)**, 1063
Simón-Díaz S., Herrero A., Uytterhoeven K., Castro N., Aerts C., Puls J., 2010, *ApJL*, **720(2)**, L174
Smith N., 2017, *Philosophical Transactions of the Royal Society of London Series A*, **375(2105)**, 20160268
Sterken C., 1977, *A&A*, **57**, 361
Torres A. F., Cidale L. S., Kraus M., Arias M. L., Barbá R. H., Maravelias G., Borges Fernandes M., 2018, *A&A*, **612**, A113
Waelkens C., Aerts C., Kestens E., Grenon M., Eyer L., 1998, *A&A*, **330**, 215
Weis K., 2011, C. Neiner, G. Wade, G. Meynet, and G. Peters (eds.), *Active OB Stars: Structure, Evolution, Mass Loss, and Critical Limits*, Vol. 272, pp 372–377
Weis K., Bomans D. J., 2020, *Galaxies*, **8(1)**, 20
West R. M., Lauberts A., Jorgensen H. E., Schuster H. E., 1987, *A&A*, **177**, L1
Yadav A. P., Glatzel W., 2016, *MNRAS*, **457(4)**, 4330